

# RSC Advances



This is an *Accepted Manuscript*, which has been through the Royal Society of Chemistry peer review process and has been accepted for publication.

*Accepted Manuscripts* are published online shortly after acceptance, before technical editing, formatting and proof reading. Using this free service, authors can make their results available to the community, in citable form, before we publish the edited article. This *Accepted Manuscript* will be replaced by the edited, formatted and paginated article as soon as this is available.

You can find more information about *Accepted Manuscripts* in the [Information for Authors](#).

Please note that technical editing may introduce minor changes to the text and/or graphics, which may alter content. The journal's standard [Terms & Conditions](#) and the [Ethical guidelines](#) still apply. In no event shall the Royal Society of Chemistry be held responsible for any errors or omissions in this *Accepted Manuscript* or any consequences arising from the use of any information it contains.

**Influence of hydrotropic coions on the shape transitions of sodium dioctylsulfosuccinate aggregates in aqueous medium†**

U. Thapa,<sup>a</sup> D. Ray,<sup>b</sup> J. Dey,<sup>a</sup> N. Sultana,<sup>a</sup> V. K. Aswal,<sup>b</sup> and K. Ismail<sup>\*a</sup>

<sup>a</sup> Department of Chemistry, North-Eastern Hill University, Shillong – 793022, India

<sup>b</sup> Solid State Physics Division, Bhabha Atomic Research Centre, Trombay, Mumbai – 400085, India

**Address for Manuscript Correspondence:** Prof. K. Ismail, Department of Chemistry, North-Eastern Hill University, NEHU Campus, Shillong - 793022, India.  
E-mail: [kismail@nehu.ac.in](mailto:kismail@nehu.ac.in); [kinchu@hotmail.com](mailto:kinchu@hotmail.com), Telephone: 91-364 – 2722610, Fax: 91-364 – 2550486

†Electronic supplementary information available: Plots of experimental surface tension values (Figs. S1-S4), experimental EMF data (Figs. S5-S6) and critical micelle concentration values (Table S1).

## Abstract

The effect of hydrotropic organic coions on the physicochemical behavior of ionic surfactants has not yet been understood clearly, although as counterions they are known to have remarkable effect on the microstructures of ionic surfactants. In this paper therefore the aggregation behavior of sodium dioctylsulfosuccinate (AOT) has been studied in aqueous media in the presence of sodium benzoate (NaB) / sodium salicylate (NaSa) / sodium meta-hydroxybenzoate (Na-mHB) / sodium para-hydroxybenzoate (Na-pHB). Surface tension and small angle neutron scattering (SANS) techniques are mainly used. AOT is known to have a special counterion binding behavior (SCB) with respect to sodium counterion, viz., at about  $0.015 \text{ mol kg}^{-1}$  of added NaCl the counterion binding constant of AOT increases suddenly by two fold which is attributed to the shape change of the AOT micelle. The SCB of AOT is found to exist in the presence of benzoate, m-hydroxybenzoate and p-hydroxybenzoate coions, but not in the presence of o-hydroxybenzoate (salicylate) coion. The SANS data, on the other hand, showed that shape transition of AOT aggregate takes place in the presence of all the four hydrotropic coions; the concentration of NaSa required to induce shape transition was however higher. Sharp increase in the value of hydrodynamic diameter determined by the dynamic light scattering (DLS) experiments also indicate shape transition of AOT aggregate in the presence of the salts. Chemical shift values of benzoate and hydroxybenzoates confirmed the binding of these coions to AOT micelle. The binding of salicylate coion is shown to be stronger due to its low hydration energy and high  $\text{pK}_h$  ( $K_h$  is the hydrolysis constant) values.

## Introduction

In aqueous solution, surfactants self-assemble into a variety of spatially organized nanostructures such as micelles, vesicles and lamellae. In the case of an ionic surfactant, the area per polar head group at the surface of a surfactant aggregate depends strongly on the nature of the counterion and more specifically on its ability to bind to the surfactant aggregate. Therefore, an easy method to induce morphological transition in surfactant aggregates is by adding counterions, since added counterions decrease the effective area per head group by screening the repulsive interaction between the head groups. Organic counterions,<sup>1-3</sup> acting mostly as hydrotropes, are found to be more effective than inorganic counterions<sup>4-6</sup> in promoting surfactant aggregation as well as morphological transition in surfactant aggregates. The structural features of hydrotropic salts are similar to surfactants since an aromatic group (hydrophobic) and an ionic group (hydrophilic) coexist within a molecule of a hydrotrope. The hydrophobicity of a hydrotrope is however generally much less than that of a surfactant. Some examples of common hydrotropic salts are benzoate, salicylate, tosylate, naphthalenesulfonate, etc. The basic hydrotropic effect refers to the property of hydrotropes to enhance the solubility of organic/biological molecules in water.<sup>7-8</sup> Studies are still being made on the physical chemistry of solutions of hydrotropes in order to obtain a better understanding of the hydrotropic effect.<sup>9</sup> Apart from studying the solubility enhancing effect of hydrotropes, study on the effect of hydrotropes on surfactant solutions is also being carried out because hydrotropes find their use in surfactant formulations. Most of the studies on the effect of hydrotropes on surfactant solutions were mainly focussed on investigating the formation of viscoelastic wormlike/entangled micelles<sup>10,11</sup> for the very fact that

such highly viscous solutions have versatile applications.<sup>12,13</sup> Studying the effect of organic/hydrophobic/hydrotropic counterions on the surfactant solutions has been gaining more importance in recent years.<sup>14-34</sup>

Both electrostatic and hydrophobic interactions contributed to the binding of organic counterions to micelles. Hydrophobic interaction can as well cause binding of organic coions to ionic micelles and as a consequence organic coions can also be expected to influence the characteristics of surfactant aggregates significantly. However, fewer studies have been made on the influence of organic coions on surfactant systems.<sup>35-41</sup> Therefore, our objective in this paper is to investigate the effect of organic coions on the aggregation and adsorption behavior of ionic surfactants.

Salicylate ion is known to have interesting effects on surfactant aggregates. Cetylpyridinium chloride/bromide (CPC/CPB) + sodium salicylate (NaSa) and cetyltrialkylammonium chloride/bromide (CTAAC/CTAAB) + NaSa systems are reported<sup>42-45</sup> to exhibit viscoelasticity in aqueous medium due to the formation of wormlike micelles. On the other hand, sodium benzoate (NaB), sodium meta-hydroxy benzoate (Na-mHB) and sodium para-hydroxy benzoate (Na-pHB) do not induce viscoelasticity in CPC/CTAAC/CTAAB system. Thus, the specificity of the hydroxyl group at ortho position in NaSa plays a decisive role in forming wormlike micelles. Sodium dioctylsulfosuccinate (AOT), a double chained anionic surfactant, has a special counterion binding behavior (SCB)<sup>46</sup> in aqueous NaCl solution, which is attributed to the shape change of the AOT micelle.<sup>47</sup> Interestingly, in the presence of salicylate ion AOT does not exhibit SCB.<sup>47,48</sup>

In view of these interesting observations, we have chosen for the present study AOT as the ionic surfactant and benzoate, meta-, para- and ortho- hydroxy benzoate as the coions.

### Experimental Section

AOT (Sigma, 99% assay), NaSa (Fluka, 99.5% assay), NaB (Fluka, 99.5% assay) were used without further purification. Na-mHB and Na-pHB were prepared from their corresponding acids (meta-hydroxybenzoic acid and para- hydroxybenzoic acid, Himedia, 99.0% assay) by neutralising them with  $\text{NaHCO}_3$ . Stock solutions of AOT and the salts were prepared in Milli-Q water, and the required concentrations were obtained by dilution.

Surface tension measurements were made by the Wilhelmy plate method using a Krüss K11 tensiometer attached with a thermostat (Haake DC 10). EMF measurements were made using Orion Dual Star ion meter and Orion 8611 BNWP sodium selective combined electrode. All measurements were taken at 25 °C. The SANS measurements were carried out at Dhruva reactor, Bhabha Atomic Research Center, Mumbai, India. In this facility, the SANS diffractometer uses a beryllium oxide filtered neutron beam of mean wavelength ( $\lambda$ ) 5.2 Å and the data were collected within the wave vector transfer ( $Q = 4\pi\sin(\theta/2)/\lambda$ , where  $\theta$  is the scattering angle) range of 0.017-0.35 Å<sup>-1</sup>. To access low-Q data some of the measurements were done at SANS-I facility, Swiss Spallation Neutron source SINQ, Paul Scherrer Institut, Switzerland. Data were collected at two sample-to-detector distances (2 and 8 m) to cover a Q range of 0.006-0.25 Å<sup>-1</sup>. Here, the wavelength of neutron beam was 6 Å and the scattered neutrons from the samples were detected using two dimensional 96 cm x 96 cm detector.<sup>49</sup> At both the facilities, the solutions were prepared in D<sub>2</sub>O (99.4 atom % D). The samples were

placed in a quartz cell having a tightly fitting Teflon stopper. The concentration of AOT was fixed at 15 mmol kg<sup>-1</sup> (mM) while the concentrations of the salts were varied. The measured SANS data were corrected to the background, the empty cell scattering and the sample transmission, and the corrected data were then normalized to the absolute cross-sectional unit using standard protocols.

The analysis of the SANS data was done according to the procedure described elsewhere.<sup>47,50</sup> In this method of data analysis, the differential scattering cross section per unit volume ( $d\Sigma/d\Omega$ ) is given by the expression

$$d\Sigma/d\Omega = n(\rho_m - \rho_s)^2 V^2 [ \langle F^2(Q) \rangle + \langle F(Q) \rangle^2 (S(Q) - 1) ] + B \quad (1)$$

In eqn (1),  $\rho_m$  and  $\rho_s$  denote the scattering length densities of the micelle and the solvent, respectively,  $n$  is the number density of the micelles,  $V$  is the volume of the micelle,  $F(Q)$  is the single particle form factor,  $S(Q)$  is the inter-particle structure factor and  $B$  is a constant term.  $F(Q)$  depends on the shape and size of the particles and  $S(Q)$  is decided by the spatial distribution of the particles.  $B$  accounts for the incoherent scattering background that occurs in the case of neutrons mainly due to the presence of hydrogen in the sample. The relations used for prolate ellipsoidal micelles are

$$\langle F^2(Q) \rangle = \int_0^1 F(Q, \mu)^2 d\mu \quad (2)$$

$$\langle F(Q) \rangle^2 = \left[ \int_0^1 F(Q, \mu) d\mu \right]^2 \quad (3)$$

$$F(Q, \mu) = 3(\sin x - x \cos x)/x^3 \quad (4)$$

$$x = Q [ a^2 \mu^2 + b^2 (1 - \mu^2) ]^{1/2} \quad (5)$$

In eqn (5),  $a$  and  $b$  are the semimajor and semiminor axes of the ellipsoidal micelle, respectively. The term  $\mu$  in the above equations refer to the cosine of the angle between the directions of  $a$  and  $Q$ . The expression for  $S(Q)$  is given by the Fourier transform of the radial distribution function  $g(r)$ .  $g(r)$  gives the probability of finding the centre of another micelle at a distance  $r$  from the centre of a reference micelle.  $S(Q)$  is calculated using the mean spherical approximation developed by Hayter and Penfold.<sup>51</sup> For vesicles having inner radius  $R$  and thickness  $dR$ , the relations used are

$$F(Q) = \frac{16\pi^2}{9} (\rho_m - \rho_s)^2 P(Q, R)$$

$$P(Q, R) = \left[ (R + dR)^3 \frac{\sin Q(R + dR) - Q(R + dR)\cos Q(R + dR)}{Q^3(R + dR)^3} - R^3 \frac{\sin QR - QR\cos QR}{Q^3R^3} \right]^2 \quad (6)$$

For a rod-like structure of radius  $R$  and length  $2l$ ,  $F(Q)$  is given by the relation

$$F(Q) = (\pi R^2 l)^2 \int_0^{\pi/2} \frac{\sin^2(Ql\cos\beta)}{(Ql\cos\beta)^2} \frac{4J_1^2(QR\cos\beta)}{(QR\cos\beta)^2} \sin\beta d\beta \quad (7)$$

where  $J_1(QR\sin\beta)$  is the first order Bessel function and  $\beta$  is the angle between the axis of the rod and  $Q$ .

Dynamic light scattering (DLS) measurements were made at 25 °C using a Malvern Zetasizer Nano ZS instrument operating at 633 nm (4 mW He-Ne laser was used) and 90° scattering angle. Samples were filtered through a 0.22 μm membrane filter prior to measurements. The scattering intensity data were processed using the instrumental software to obtain the hydrodynamic diameter ( $d_H$ ) of aggregates in each sample.



$^1\text{H}$  NMR spectra of the salt solutions in the absence and presence of AOT in  $\text{D}_2\text{O}$  (Aldrich, 99.9% D atom) were recorded at 25 °C on a Bruker Advance II-400 Spectrometer operating at 400 MHz.

## Results and Discussion

Representative plots of the surface tension ( $\gamma$ ) versus AOT concentration in the presence of varying concentrations of NaB are shown in Figs. S1-S4. The values of critical micelle concentration (cmc) determined from the surface tension isotherms are shown in Fig. 1 (Table S1) as a function of the salt concentration.

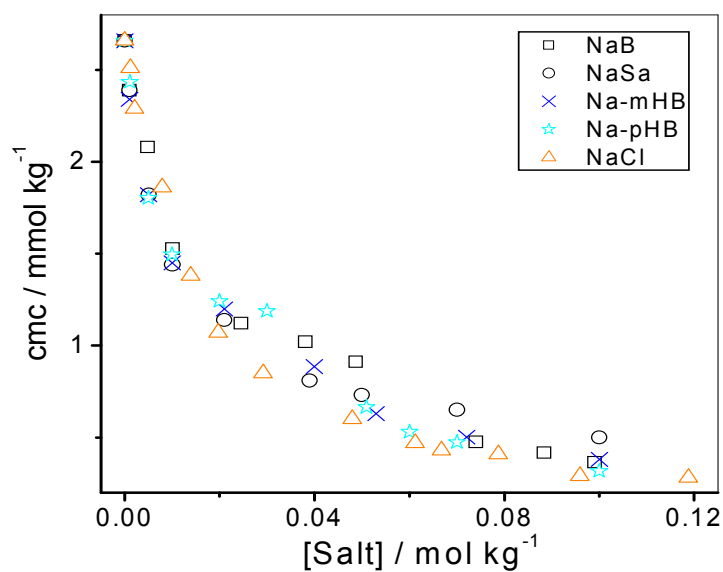


**Fig. 1.** Variation of cmc of AOT as a function of salt concentration. Cmc values of AOT in the presence of NaCl were taken from reference 46.

## Counterion Binding

From Fig. 2, it is apparent that the effect of the benzoate and hydroxybenzoate coions on the cmc of AOT is not very significant. To determine the counterion

binding constant ( $\beta$ ) of AOT in the aqueous salt media, we have used the Corrin-Harkins (CH) equation,

$$\ln c_0 = A - \beta[\ln(c_0 + c_e)] \quad (8)$$

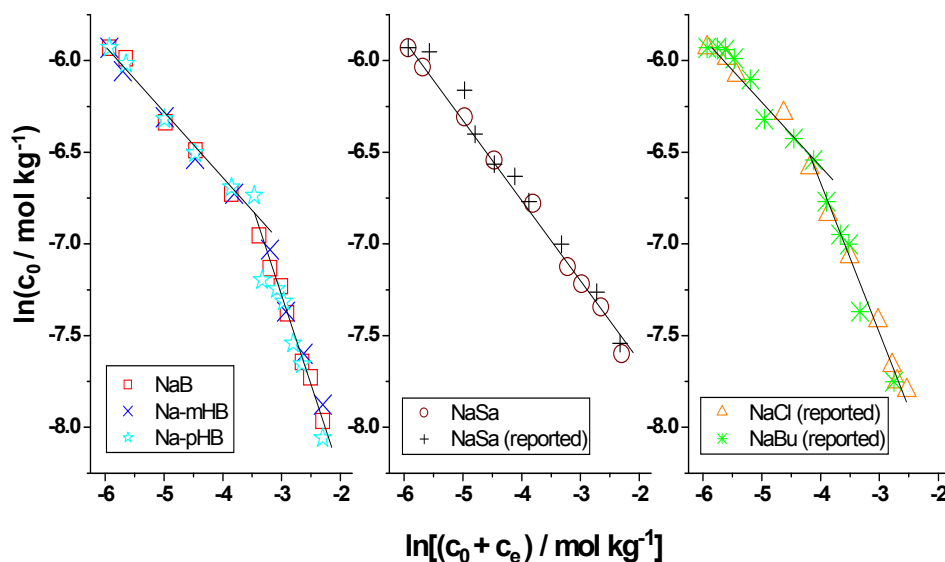


**Fig. 2.** CH plots of AOT in different salt medium. The data for AOT+NaCl and AOT+NaBu (sodium butyrate) are taken from reference 46 and those for AOT+NaSa are taken from reference 48.

where  $c_0$  is the cmc,  $c_e$  is the concentration of the added hydrotrope and  $A$  is a constant related to the free energy of micellization. The CH plots are shown in Fig. 2 and they reveal the influence of coions on the SCB of AOT. The SCB of AOT refers to a sudden change in the value of  $\beta$  at a certain concentration of added salt. As apparent from Fig. 2, the SCB of AOT exists in the presence of benzoate, m-hydroxybenzoate and p-hydroxybenzoate coions, but as observed earlier<sup>47,48</sup> not in the presence of salicylate coion. The value of  $\beta$  and the

concentration of salt ( $c^*$ ) at which the  $\beta$  value abruptly increases are determined from Fig. 2 and given in Table 1. In the case of the three aromatic coions, viz., benzoate, m-hydroxybenzoate and p-hydroxybenzoate, the  $c^*$  increased to 30 mM ( $M = \text{mol kg}^{-1}$ ) from 15 mM found in the presence of NaCl and sodium butyrate (NaBu).<sup>46</sup> Thus, the aromatic coions increase the value of  $c^*$ . The value of  $\beta$  also has been found to change to a certain extent in the presence of organic coions. The position of the hydroxyl group appears to have negligible effect on  $c^*$ , since  $c^*$  value is found to be same in the presence of benzoate, m-hydroxybenzoate and p-hydroxybenzoate coions. On the other hand, the influence of o-hydroxybenzoate (salicylate) coion on the SCB is entirely different and so significant that the SCB disappears, in other words,  $c^*$  increases to very high value.

In order to measure the amount of sodium ions bound to AOT micelle, we also determined the cmc from the EMF method using sodium ion-selective electrode. The experimental EMF data are shown for AOT in the presence of NaB and Na-PHB in Figs. S5 and S6, respectively. These data were analyzed in the fashion described earlier<sup>46</sup> and the value of  $\beta$  was determined using an iteration method. We could determine the values of cmc and  $\beta$  only up to 30 mM salt concentration (values shown in Figs. S5 and S6), which are comparable to the values obtained above from the surface tension data and the CH plot. However, the values of cmc and  $\beta$  could not be determined accurately above 30 mM salt concentration because the EMF data were found to be scattered and not reproducible. Probably high background concentration of sodium counterion in the salt solution is responsible for this, because addition of low concentration of AOT to such a salt solution may not produce much change in the EMF.

As stated in the introduction section, in CPC/CPB/CTAAC/CTAAB surfactants viscoelasticity is induced by the salicylate counterion, but not by the benzoate, m-hydroxybenzoate and p-hydroxybenzoate counterions. Analogously, there is a distinction between the influence exerted by benzoate, m-hydroxybenzoate and p-hydroxybenzoate coions on the SCB of AOT on one hand and that by salicylate coion on the other hand. Therefore, with respect to inducing viscoelasticity in CPC/CPB/CTAAC/CTAAB surfactants and influencing the SCB of AOT, the salicylate ion (as counterion or coion) behaves differently compared to other isomeric hydroxybenzoates. The present study therefore reveals that the effect of ortho-hydroxybenzoate (salicylate) on the binding of sodium counterion to anionic AOT micelle is different from that of meta- and para- isomers. The neutron reflectivity study<sup>52</sup> on the adsorption of hydroxybenzoate and chlorobenzoate counterions at the CTAB monolayer – water interface also revealed that the degree of counterion binding and the location of the counterions are not same for the different isomeric forms of these counterions.

The difference in the counterion binding behavior of AOT in aqueous NaSa as compared to that in aqueous NaB, Na-mHB and Na-pHB reveals that the location and orientation of salicylate coion bound to the AOT micelle is different from those of the other three coions. This may be explained in the following manner:

The  $pK_a$  ( $K_a$  is the dissociation constant) values for the different benzoates<sup>53</sup> are: NaB, 4.19; NaSa, 2.97; Na-mHB, 4.06; Na-pHB, 4.48. Since we are dealing with the salts of these acids, the benzoate and the hydroxybenzoate ions undergo hydrolysis in aqueous medium. The  $pK_h$  ( $K_h$  is the hydrolysis constant) values of salicylate, benzoate, m-hydroxybenzoate and p-

hydroxybenzoate ions are therefore equal to 11.03, 9.81, 9.94 and 9.52, respectively. Salicylate ions thus undergo least hydrolysis, which may be correlated to the presence of strong intramolecular hydrogen bonding in this ion. Shapley et al.<sup>53</sup> showed that there is a strong intramolecular hydrogen bonding in salicylate ion due to which it has lowest solvation energy, about 8 – 10 kcal/mol lower than that of benzoate, which is in agreement with its high value of  $pK_h$ . Low hydration energy and high  $pK_h$  value render salicylate ion more hydrophobic than benzoate, m-hydroxybenzoate and p-hydroxybenzoate, and this characteristic of salicylate ion is considered to be responsible for its strong binding to cationic (as counterion) as well as to anionic (as coions) micelles.

#### **SANS measurements**

It was shown in the earlier study<sup>47,50,54</sup> that the shape change of AOT micelle is responsible for the abrupt change in the value of  $\beta$  in aqueous NaCl,  $NH_4Cl$  and tetraalkylammonium bromide solutions. The effect of the four organic coions on the shape/morphological transition of AOT aggregates is discussed below on the basis of the SANS data. In SANS experiments, the differential scattering cross section per unit volume ( $d\Sigma/d\Omega$ ) as a function of  $Q$  is measured. The different equations used in the determination of the shape of aggregates are given elsewhere.<sup>47,50</sup>

**AOT + NaB + D<sub>2</sub>O System.** The SANS data for the 15 mM AOT solution with varying concentration (10-70 mM) of the added NaB are shown in Fig. 3. At 10 mM concentration of added NaB, the data is found to be best fitted with ellipsoidal model and the fitted micellar parameters are given in Table 2. A strong increase in the scattering at low  $Q$  is observed at 15 mM of added NaB concentration. Such a scattering profile is found to have a slope of -1 when plotted

in log-log scale, which primarily indicates transformation to rod-like morphology of AOT (Table 3). The scattering intensity of AOT at 20 mM of added NaB increases further and shows best agreement with the model in which both rod-like micelles and unilamellar vesicles (ULV) co-exist. On increasing the concentrations of NaB to 30-70 mM, the scattering increased further and the data is best described in terms of vesicles + rods model. The values of the parameters obtained from these fittings are shown in Table 3. Thus, added NaB induces microstructural change of AOT aggregates from prolate ellipsoid to rods to rods + vesicles.

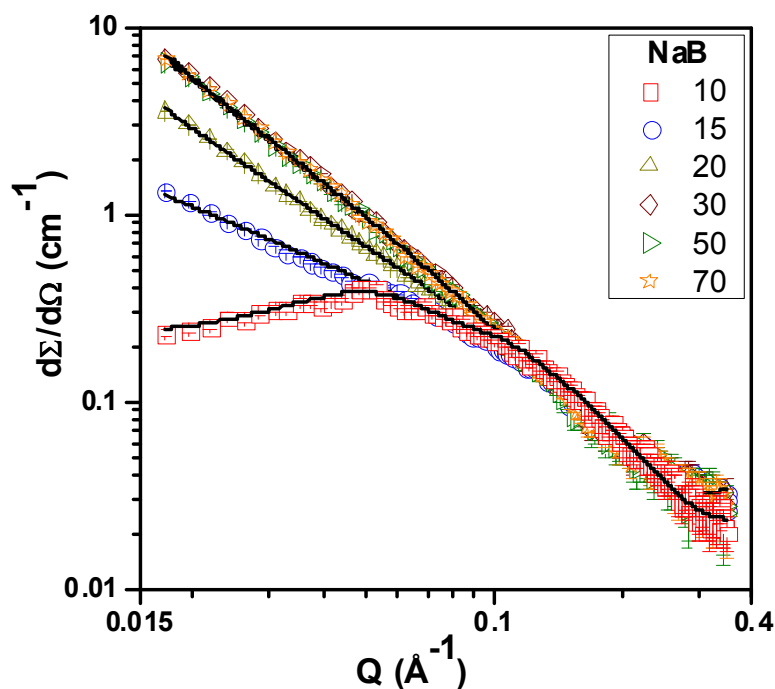


**Fig. 3.** Plots of SANS data (differential scattering cross section per unit volume versus scattering vector  $Q$ ) for AOT (15 mM) in the presence of different concentrations of NaB (in mM shown in inset). The black lines are model fits.

**AOT + Na-mHB + D<sub>2</sub>O and AOT + Na-pHB + D<sub>2</sub>O Systems.** The SANS data for the 15 mM AOT solution with varying concentration (10-70 mM) of the added Na-mHB and Na-pHB are shown in Fig. 4. The scattering curves of AOT in the presence of 10 mM of added Na-mHB or Na-pHB are found to be best fitted with the prolate-ellipsoidal model. The parameters associated with it are given in Table 2. The scattering intensity of AOT at low Q increases suddenly at 15 mM of added Na-mHB or Na-pHB. The scattering data of 15 mM AOT + 15 mM Na-mHB system were found to be best fitted with the rod-like micelle model, whereas the data corresponding to 15 mM AOT + 15 mM Na-pHB system are best fitted with the model in which both rod-like micelles and vesicles co-exist. The scattering data of AOT with 20-70 mM of added Na-mHB or Na-pHB show similarity and these data fit best with the model in which both rods and vesicles co-exist. The parameters of the fitting are given in Table 3. Thus, similar to NaB, from 20 mM concentration onward Na-mHB and Na-pHB too induce similar morphological transition of AOT aggregates.

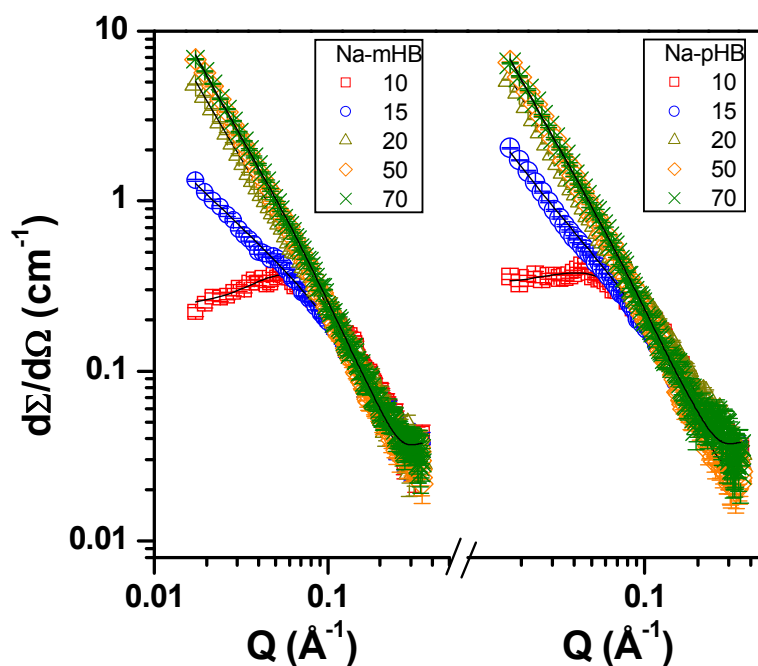


**Fig. 4.** Plots of SANS data (differential scattering cross section per unit volume versus scattering vector  $Q$ ) for AOT (15 mM) in the presence of different concentrations of Na-mHB and Na-pHB (in mM shown in inset). The black lines are model fits.

**AOT + NaSa + D<sub>2</sub>O System.** The scattering profiles of AOT in presence of increasing concentrations of NaSa are shown in Fig. 5. For pure 15 mM AOT, the scattering is consistent with prolate ellipsoid type of structure based on model fitting and is in agreement with our earlier report.<sup>47</sup> SANS data of 15 mM AOT + 15 mM NaSa showed no change in the shape of AOT aggregates, which is also in complete agreement with our earlier report.<sup>47</sup> However, when the SANS measurements were made on systems containing 15 mM AOT and NaSa concentration equal or more than 20 mM, then we could surprisingly see that the scattering intensity at the lower  $Q$  regime increases and the correlation peak



disappears (Fig. 5). When NaSa concentration is 20 mM, the SANS data were best fitted to the model in which both rods and vesicles co-exist (Table 3). At 50 and 100 mM of added NaSa, the scattering by AOT follows a linear pattern on log-log scale with slope equal to almost -2 and the SANS data were best fitted to the unilamellar vesicle model (Table 3). Hence, morphology of AOT aggregates undergoes transition when the amount of added NaSa becomes  $\geq 20$  mM. Thus, it can be concluded that even in the presence of NaSa shape transition of AOT aggregate takes place but at a higher concentration of NaSa compared to other salts under consideration.

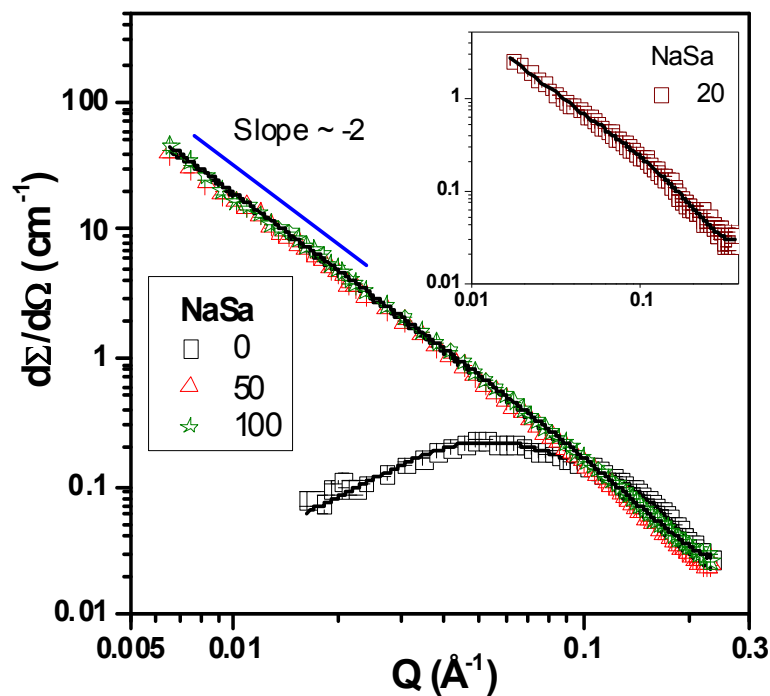


**Fig. 5.** Plots of SANS data (differential scattering cross section per unit volume versus scattering vector  $Q$ ) for AOT (15 mM) in the presence of different concentrations of NaSa (in mM shown in inset). The black lines are model fits.

Thus, SANS data clearly reveal that the AOT aggregates in the presence of added NaB/NaSa/Na-mHB/Na-pHB undergo a shape transition irrespective of the fact that whether –OH group is absent or present or the position of the –OH group is different. Referring to our previous SANS data of AOT in presence of added NaCl, the shape transition of AOT aggregate takes place at 15 mM of added NaCl and a sudden two-fold change in the slope of the CH plot also takes place at almost the same concentration, i.e., 15 mM NaCl. Such a correlation found earlier<sup>47</sup> between the shape change of AOT aggregate and the sudden change in the slope of the CH plot appears to have a dependence on the coions present in the system. In the cases of NaB, Na-mHB and Na-pHB, AOT has two values of  $\beta$  and SANS data too shows morphology change of AOT aggregate. From the SANS data, the shape change of AOT aggregate appears to occur at a lower salt concentration (15 mM) than expected from the  $c^*$  (30 mM of salt concentration) value. However, this discrepancy disappears when we consider the total sodium ion (counterion) concentration at the region of shape change. The total sodium ion concentration is the sum of sodium ions contributed by the surfactant and the salt. The results of the CH plot refer to the behavior of the micellar system at the cmc (because the CH equation is valid at the cmc). At  $c^* = 30$  mM, the total sodium counter ion concentration is equal to about 31 mM (Sodium ion contributed by AOT is about 1 mM since this is the cmc value of AOT in the presence of 30 mM of added salt). In SANS measurements the concentration of AOT needs to be kept high to get good neutron scattering, because at the cmc the scattering of neutron is very poor. Therefore, the AOT concentration is kept 15 mM in SANS experiments and the total sodium counter ion concentration at the region where micellar shape change takes place in the

presence of benzoate and hydroxybenzoates is nearly equal to 30 mM (35 mM in the presence of NaSa). Thus, there is a good correlation between the CH plot result and SANS result with respect to total sodium ion concentration in presence of benzoate, m-hydroxybenzoate and p-hydroxybenzoate. In the case of NaSa, major discrepancy is however observed since the CH plot of AOT in presence of added NaSa shows only one region of counterion binding indicating thereby no shape change of AOT micelle. On the contrary, SANS data show two different morphologies of AOT aggregate in the presence of 20 mM or more of NaSa. Thus, NaSa is an exception as far as the correlation between slope change of the CH plot and shape change of AOT aggregate is concerned.

As we add sodium salt to a micellar solution of AOT, more counterions bind to a micelle (number of bound counterions,  $m$ , increases) which reduces the repulsion between the head groups at the micellar surface thereby increasing the aggregation number ( $n$ ). Increase in aggregation number increases the size of the micelle, but the value of  $\beta$  remains almost unchanged since it is equal to the ratio ( $m/n$ ) of the bound counterions to the aggregation number. Thus, although the values of both  $m$  and  $n$  increases when sodium salt is added, fortuitously the ratio  $m/n$  or  $\beta$  remains constant. However, as  $n$  increases size increases and at some point the shape also changes due to geometric requirement.<sup>47</sup> At this point, the ratio  $m/n$  takes a different value and  $\beta$  changes. This is one explanation for correlating change in  $\beta$  to the shape change of micelle.<sup>47</sup> In the light of this, it may be visualized that in the presence of NaSa although AOT micelle changes shape at about 20 mM concentration of NaSa, the value of  $\beta$  does not change because even after the micellar shape change the values of  $m$  and  $n$  may still be changing in

such a manner that no change in the value of the ratio  $m/n$  occurs unlike in the case of NaCl, NaB, Na-mHB and Na-pHB.

The salicylate, benzoate, m-hydroxybenzoate and p-hydroxybenzoate ions after binding to the micelle may be considered to reside at the Stern layer. Stern layer now becomes a compact layer of polar headgroups ( $-\text{SO}_3^-$  and  $-\text{COO}^-$ ). In the case of salicylate the  $-\text{OH}$  group may also reside near the Stern layer. The surface potential thus increases. Because of the intramolecular hydrogen bonding salicylate may bind more strongly compared to other ions as already mentioned above. However, in the case of benzoate, m-hydroxybenzoate and p-hydroxybenzoate the surface potential increase will be more and consequently more sodium counterions will bind. Such differences in the binding of salicylate ion due to intramolecular hydrogen bonding may be responsible for the different counterion ion binding behavior in the presence of salicylate.

### **DLS measurements**

In order to confirm further the variation of the morphology of AOT aggregate at some critical concentrations of added counterions, we performed DLS measurements of 15 mM AOT solutions with varying amounts of NaB and NaSa. In Fig. 6 the variation of  $d_H$  of AOT aggregate is shown as a function of concentration of NaB and NaSa. A sudden increase in  $d_H$  (about 1.6 times) occurs at a salt concentration which is comparable to the salt concentration where morphological transition has been found to occur from the SANS data. We expect same behavior with AOT + Na-mHB and Na-pHB also. The sudden change in  $d_H$  confirms the change in the morphology of AOT at a particular concentration of the added salt as revealed by the SANS data.

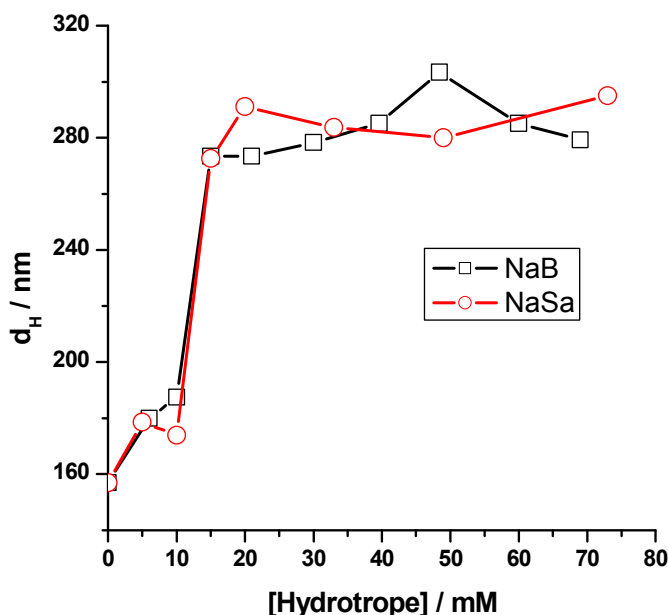


**Fig. 6.** Variation of hydrodynamic diameter of AOT (15 mM) with hydrotrope concentration.

### <sup>1</sup>H NMR Spectra

The chemical shift ( $\delta$ ) values of the benzoate and hydroxybenzoates are listed in Table 4. Whatever the isomer may be, the trend in the  $\delta$  value with increase in the salt concentration as we go from pre-micellar to micellar region is the same. In presence of micelle, the  $\delta$  values remain constant irrespective of the concentration of the salt above  $c^*$ . For all the protons of benzoate, an overall increase in the chemical shift (deshielding) is observed in AOT micellar medium irrespective of the positions of the protons. The deshielding of the benzoate protons suggest that the benzoate ions move from polar solvent medium ( $D_2O$ ) to less polar stern layer region of the AOT micelle.<sup>55</sup> Similar trends in the variation of  $\delta$  were observed in

the case of other coions also. Thus,  $^1\text{H}$  NMR spectra confirm the binding of benzoate and hydroxybenzoate coions to the AOT micelle.

### Conclusions

In aqueous AOT solution, added organic coions like benzoate, ortho-hydroxybenzoate (salicylate), meta-hydroxybenzoate and para-hydroxybenzoate bind to the AOT micelle. This binding of coions is attributed to hydrophobic interaction and it affects significantly the binding of sodium counterion to AOT micelle and also the morphological transition of AOT micelles. The CH plots revealed the SCB of AOT existing in the presence of NaB, Na-mHB and Na-pHB and its disappearance in the presence of NaSa, whereas the SANS data showed the shape transition of AOT aggregate taking place in the presence of all the four salts (NaB, NaSa, Na-mHB and Na-pHB). In the presence of NaB, Na-mHB and Na-pHB the shape transition occurred from prolate ellipsoids to rods to rods + vesicles as the concentration of the salt increased. The concentration of NaB / Na-mHB / Na-pHB at which prolate ellipsoid to rod transition of AOT aggregate takes place is 15 mM which is same as that found in the presence of NaCl.<sup>47</sup> On the other hand, slope change of the CH plots of AOT takes place in the presence of 30 mM ( $c^*$ ) of NaB, Na-mHB and Na-pHB. Thus, benzoate, meta-hydroxybenzoate and para-hydroxybenzoate coions increase the value of  $c^*$  to 30 mM, which was otherwise 15 mM in the presence of NaCl. In other words, these three coions suppress the SCB of AOT to a certain extent, but not completely (complete suppression of SCB can be considered as equivalent to  $c^* \rightarrow \infty$ ). Unlike these three coions, salicylate coion suppresses the SCB of AOT completely. But, SANS data showed occurrence of shape change of AOT micelle in the presence of NaSa also when the amount of NaSa is  $\geq 20$  mM instead of 15

mM as in the case of NaB, Na-mHB and Na-pHB. The present study therefore provides further support to the inference that slope change of the CH plot is an indication of the occurrence of shape change of AOT micelle, but also reveals that salicylate coion behaves differently by causing shape change of AOT micelle without manifesting any change in the slope of CH plot.

### **Acknowledgment**

We acknowledge the financial support received from the DST, New Delhi and UGC, New Delhi. U. T. and N. S. acknowledge the UGC, New Delhi for the research fellowships. J.D. acknowledges the CSIR, New Delhi for the Research Associateship.

## References

1. P. A. Hassan, R. R. Srinivasa and E. W. Kaler, *Langmuir*, 2002, **18**, 2543-2548.
2. P. A. Hassan, G. Fritz and E. W. Kaler, *J. Colloid Interface Sci.*, 2003, **257**, 154-162.
3. G. Garg, P. A. Hassan, V. K. Aswal and S. Kulshreshtha, *J. Phys. Chem. B*, 2005, **109**, 1340-1346.
4. M. Bergström and J. S. Pedersen, *Phys. Chem. Chem. Phys.*, 1999, **1**, 4437-4446.
5. M. Almgren, J. C. Gimel, K. Wang, G. Karlsson, K. Edwards, W. Brown and K. Mortensen, *J. Colloid Interface Sci.* 1998, **202**, 222-231.
6. L. J. Magid, Z. Li and P.D. Butler, *Langmuir* 2000, **16**, 10028-10036.
7. H. S. Booth and H. E. Everson, *Ind. Eng. Chem. Ind. Ed.*, 1948, **40**, 1491-1493.
8. A. M. Saleh and L. K. El-Khordagui, *Int. J. Pharm.* 1985, **24**, 231-238.
9. J. Eastoe, M. H. Hatzopoulos and P. J. Dowding, *Soft Matter*, 2011, **7**, 5917-5925.
10. M. E. Cates and S. J. Candau, *J. Phys. Condens. Matter*, 1990, **2**, 6869-6892.
11. T. M. Clausen, P. K. Vinson, J. R. Minter, H. T. Davis, Y. Talmon and W. G. Miller, *J. Phys. Chem.*, 1992, **96**, 474-484.
12. L. M. Walker, *Curr. Opin. Colloid Interface Sci.* 2001, **6**, 451-456.
13. M. J. Rosen and M. Dahanayake, AOCS Press, Champaign, Illinois, **2000**.
14. R. Abdel-Rahem, *Adv. Colloid Interface Sci.*, 2008, **141**, 24-36.



15. W. Ge, E. Kesselman, Y. Talmon, D. J. Hart and J. L. Zakin, *J. Non-Newtonian Fluid Mech.* 2008, **154**, 1-12.
16. J. Penfold, I. Tucker, E. Staples and R. K. Thomas, *Langmuir* 2004, **20**, 8054-8061.
17. D. Yu, M. Tian, Y. Fan, G. Ji and Y. Wang, *J. Phys. Chem. B*, 2012, **116**, 6425-6430.
18. W-J. Kim and S-M. Yang, *J. Colloid Interface Sci.*, 2000, **232**, 225-234.
19. J. Zhang, B. Dong, L. Zheng and G. Li, *Colloids Surf. A: Physicochem. Eng. Aspects*, 2006, **290**, 157-163.
20. R. Abdel-Rahem, M. Gradzielski and H. Hoffmann, *J. Colloid Interface Sci.* 2005, **288**, 570-582.
21. G. C. Kalur, B. D. Frounfelker, B. H. Cipriano, A. I. Norman and S. R. Raghavan, *Langmuir* 2005, **21**, 10998-11004.
22. T. Mukhim, J. Dey, S. Das and K. Ismail, *J. Colloid Interface Sci.* 2010, **350**, 511-515.
23. G. Garg, P. A. Hassan, V. K. Aswal and S. K. Kulshreshtha, *J. Phys. Chem. B* 2005, **109**, 1340-1346.
24. G. Garg, V. K. Aswal, S. K. Kulshreshtha and P. A. Hassan, *Pramana* 2004, **63**, 351-355.
25. P. A. Hassan, S. N. Sawant, N. C. Bagkar and J. V. Yakhmi, *Langmuir*, 2004, **20**, 4874-4880.
26. S. Kumar, Z. A. Khan and Kabir-ud-Din, *J. Surf. Deterg.*, 2004, **7**, 367-371.
27. V. K. Aswal, *J. Phys. Chem. B*, 2003, **107**, 13323-13328.
28. S. Kumar, D. Sharma and Kabir-ud-Din, *Langmuir*, 2003, **19**, 3539-3541.

29. S. Kumar, A. Z. Naqvi, V. K Aswal, P. S. Goyal and Kabir-ud-Din. *Curr. Sci.*, 2003, **84**, 1346-1349.
30. Kabir-ud-Din, S. Kumar and D. Sharma, *J. Surf. Deterg.*, 2002, **5**, 131-134.
31. M. Akram, S. Yousuf, T. Sarwar and Kabir-ud-Din, *Colloids Surf. A: Physicochem. Eng. Aspects*, 2014, **441**, 281-290.
32. J. Aslam, U. S. Siddiqui, W. H. Ansari and Kabir-ud-Din, *J. Surf. Deterg.*, 2013, **16**, 693-707.
33. M. Ali, M. Jha, S. K. Das and S. K. Saha, *J. Phys. Chem. B*, 2009, **113**, 15563-15571.
34. R. A. Abdel-Rahem, *J. Surf. Deterg.*, 2014, **17**, 353-362.
35. S. Ikeda, S. Hayashi and T. Imae, *J. Phys. Chem.*, 1981, **85**, 106-112
36. B. C. Paul, S. S. Islam, and K. Ismail, *J. Phys. Chem. B* 1998, **102**, 7807-7812.
37. R. Ranganathan, L. T. Okano, C. Yihwa, E. O. Alonso, F. H. Quina, *J. Phys. Chem. B* 1999, **103**, 1977-1981
38. T. Narita, N. Hirota, J. P. Gong, Y. Osada, *J. Phys. Chem. B* 1999, **103** 6262-6266.
39. I. M. Umlong and K. Ismail, *Colloid Surf. A* 2007, **299**, 8-14.
40. M. A. Bhat, A. A. Dar, A. Amin and G. M. Rather, *J. Disper. Sci. Technol.* 2008, **29**, 514-520
41. K. T. Nguyen and A. V. Nguyen, *Soft Matter* 2014, **10**, 6556-6563.
42. T. Shikata, H. Hirata and T. Kotaka, *Langmuir*, 1988, **4**, 354-359.
43. N. Memoto and M. Kuwahara, *Langmuir*, 1993, **9**, 419-423.

44. U. R. K. Rao, C. Manohar, B. S. Valaulikar and R. M. Iyer, *J. Phys. Chem.*, 1987, **91**, 3286-3291.
45. Narayan Ch. Das, Hu Cao, Helmut Kaiser, Garfield Warren, Joseph Gladden and Paul E. Sokol, *Langmuir*, 2012, **28**, 11962-11968.
46. I. M. Umlong and K. Ismail, *J. Colloid Interface Sci.*, 2005, **291**, 529-536.
47. J. Dey, J. Bhattacharjee, P. A. Hassan, V. K. Aswal, S. Das, and K. Ismail, *Langmuir*, 2010, **26**, 15802-15806.
48. I. M. Umlong and K. Ismail, *J. Surface. Sci. Technol*, 2006, **22**, 101-117.
49. J. Kohlbrecher and W. Wagner, *J. Appl. Cryst.*, 2000, **33**, 804-806.
50. U. Thapa, J. Dey, S. Kumar, P. A. Hassan, V. K. Aswal and K. Ismail, *Soft Matter*, 2013, **9**, 11225-11232.
51. J. B. Hayter and P. Penfold, *Mol. Phys.* 1981, **42**, 109-118.
52. J. Penfold, I. Tucker, E. Staples, R. K. Thomas, *Langmuir*, 2004, **20**, 8054-8061.
53. W. A. Shapley, G. B. Bacskay and G. G. Warr, *J. Phys. Chem. B*, 1998, **102**, 1938-1944.
54. J. Dey, U. Thapa and K. Ismail, *J. Colloid Interface Sci.*, 2012, **367**, 305-310.
55. M. Vermathen, P. Stiles, S. J. Bachofer and U. Simonis, *Langmuir*, 2002, **18**, 1030-1042.

**Figure caption**

**Fig. 1.** Variation of cmc of AOT as a function of salt concentration. Cmc values of AOT in the presence of NaCl were taken from reference 39.

**Fig. 2.** CH plots of AOT in different salt medium. The data for AOT+NaCl and AOT+NaBu (sodium butyrate) are taken from reference 39 and those for AOT+NaSa are taken from reference 41.

**Fig. 3.** Plots of SANS data (differential scattering cross section per unit volume versus scattering vector  $Q$ ) for AOT (15 mM) in the presence of different concentrations of NaB (in mM shown in inset). The black lines are model fits.

**Fig. 4.** Plots of SANS data (differential scattering cross section per unit volume versus scattering vector  $Q$ ) for AOT (15 mM) in the presence of different concentrations of Na-mHB and Na-pHB (in mM shown in inset). The black lines are model fits.

**Fig. 5.** Plots of SANS data (differential scattering cross section per unit volume versus scattering vector  $Q$ ) for AOT (15 mM) in the presence of different concentrations of NaSa (in mM shown in inset). The black lines are model fits.

**Fig. 6.** Variation of hydrodynamic diameter of AOT (15 mM) with hydrotrope concentration.

**Table 1. Values of Counterion Binding Constant ( $\beta$ ) for AOT in Aqueous Salt Solutions at 25 °C Derived from Corrin-Harkins Plot ( $c^*$  represents salt concentration in mM)**

Salt	$c^*$	$\beta$	
		below $c^*$	above $c^*$
NaCl	15.0	0.39	0.82
NaB	30.0	0.41	0.71
NaSa	-	0.45	-
Na-mHB	30.0	0.37	0.92
Na-pHB	30.0	0.32	0.95

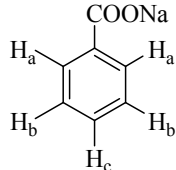
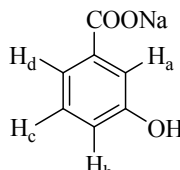
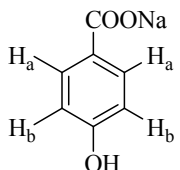
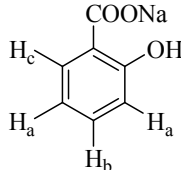
**Table 2. Micellar Parameters Obtained by Fitting SANS Data for 15 mM AOT in the Presence of Varying Concentrations of Salts Using a Prolate-ellipsoidal Model.**

Salt	Salt Conc. (mM)	Semi-major Axis (Å)	Semi-minor Axis (Å)	Fractional Charge	Aggregation Number
NaB	10	29.1 ± 0.7	12.6 ± 0.4	0.33	32
Na-mHB	10	31.2 ± 0.7	12.6 ± 0.4	0.34	34
Na-pHB	10	30.1 ± 0.7	12.6 ± 0.4	0.29	31

**Table 3. Micellar Parameters Obtained by Fitting SANS Data for 15 mM AOT in the Presence of Varying Concentrations of Salts Using Different Structural Models.**

Salt	Salt Conc. (mM)	Structure	Thickness of vesicle (Å)	Radius of rod (Å)
NaB	15	Rods	-	12.6 ± 0.4
NaB	20	Rods and ULV	17.6 ± 0.6	12.6 ± 0.4
NaB	30	Rods and ULV	17.6 ± 0.6	12.6 ± 0.4
NaB	50	Rods and ULV	17.7 ± 0.6	12.6 ± 0.4
NaB	70	Rods and ULV	17.8 ± 0.6	12.6 ± 0.4
Na-mHB	15	Rods	-	12.6 ± 0.4
Na-mHB	20	Rods and ULV	17.5 ± 0.6	12.6 ± 0.4
Na-mHB	50	Rods and ULV	17.6 ± 0.6	12.6 ± 0.4
Na-mHB	70	Rods and ULV	17.7 ± 0.5	12.6 ± 0.4
Na-pHB	15	Rods and ULV	17.6 ± 0.5	12.6 ± 0.4
Na-pHB	20	Rods and ULV	17.7 ± 0.5	12.6 ± 0.4
Na-pHB	50	Rods and ULV	17.7 ± 0.5	12.6 ± 0.4
Na-pHB	70	Rods and ULV	17.9 ± 0.5	12.6 ± 0.4
NaSa	20	Rods and ULV	17.7 ± 0.5	12.6 ± 0.4
NaSa	50	ULV	18.0 ± 0.5	-
NaSa	100	ULV	18.2 ± 0.6	-

**Table 4. Chemical Shift Values of the Protons of the Salt in Pure D<sub>2</sub>O and Micellar Media.**

System	$\delta$ / ppm			
	H <sub>a</sub>	H <sub>b</sub>	H <sub>c</sub>	H <sub>d</sub>
10 mM NaB	7.698	7.308	7.382	
20 mM NaB+10 mM AOT	7.795	7.406	7.482	
60 mM NaB+10 mM AOT	7.793	7.401	7.475	
	H <sub>a</sub>	H <sub>b</sub>	H <sub>c</sub>	H <sub>d</sub>
10 mM Na-mHB	7.216	6.843	7.179	7.234
20 mM Na-mHB+10 mM AOT	7.310	6.935	7.267	7.329
60 mM Na-mHB+10 mM AOT	7.294	6.921	7.254	7.313
	H <sub>a</sub>	H <sub>b</sub>		
10 mM Na-pHB	7.657	6.737		
20 mM Na-pHB+10 mM AOT	7.726	6.822		
60 mM Na-pHB+10 mM AOT	7.721	6.814		
	H <sub>a</sub>	H <sub>b</sub>	H <sub>c</sub>	
10 mM NaSa	6.809	7.303	7.665	
20 mM NaSa +10 mM AOT	6.893	7.388	7.749	
<b>Structures</b>				
				
NaB	Na-mHB	Na-pHB	NaSa	